

# Electrophoretic deposition of lawsone loaded bioactive glass (BG)/chitosan composite on polyetheretherketone (PEEK)/BG layers as antibacterial and bioactive coating

Muhammad Atiq Ur Rehman <sup>1</sup>, Fatih Erdem Bastan,<sup>1,2</sup> Qaisar Nawaz,<sup>1</sup> Wolfgang H. Goldmann,<sup>3</sup> Muhammad Maqbool,<sup>1</sup> Sannakaisa Virtanen,<sup>4</sup> Aldo R. Boccaccini <sup>1</sup>

<sup>1</sup>Department of Materials Science and Engineering, Institute of Biomaterials, University of Erlangen-Nuremberg, Cauerstr.6, 91058, Erlangen, Germany

<sup>2</sup>Engineering Faculty, Department of Metallurgy and Materials Engineering, Thermal Spray Research and Development Laboratory, Sakarya University, 54187, Esentepe, Sakarya, Turkey

<sup>3</sup>Department of Biophysics, Friedrich-Alexander-University, Erlangen-Nuremberg, Henkstr.91, 91052, Erlangen, Germany

<sup>4</sup>Department of Materials Science and Engineering, Chair for Surface Science of Corrosion, University of Erlangen-Nuremberg, Martenstr. 5-7, 91058, Erlangen, Germany

Received 14 May 2018; revised 24 June 2018; accepted 12 July 2018

Published online 14 September 2018 in Wiley Online Library (wileyonlinelibrary.com). DOI: 10.1002/jbm.a.36506

**Abstract:** In this study, chitosan/bioactive glass (BG)/lawsone coatings were deposited by electrophoretic deposition (EPD) on polyetheretherketone (PEEK)/BG layers (previously deposited by EPD on 316-L stainless steel) to produce bioactive and antibacterial coatings. First, the EPD of chitosan/BG/lawsone was optimized on stainless steel in terms of suspension stability, homogeneity and thickness of coatings. Subsequently, the optimized EPD parameters were used to produce bioresorbable chitosan/bioactive glass (BG)/lawsone coatings on PEEK/BG layers. The produced layered coatings were characterized in terms of composition, microstructure, corrosion resistance, in vitro bioactivity, drug release kinetics and antibacterial activity. Ultraviolet/Visible (UV/VIS) spectroscopic analyses confirmed the release of lawsone from the coatings. Moreover, the deposition of chitosan/BG coatings was confirmed by

Scanning Electron Microscopy (SEM) and Fourier Transform Infrared spectroscopy (FTIR). The coated specimens presented higher corrosion resistance (10 times) in comparison to that of bare 316-L stainless steel and showed convenient wettability for initial protein attachment. The presence of lawsone in the top layer provided antibacterial effects against *Staphylococcus carnosus*. Moreover, the developed coatings formed apatite-like crystals upon immersion in simulated body fluid, indicating the possibility of achieving close interaction between the coating surface and bone. © 2018 Wiley Periodicals, Inc. *J Biomed Mater Res Part A*: 106A: 3111–3122, 2018.

**Key Words:** electrophoretic deposition, multilayer coatings, antibacterial coatings, bioactive coatings, PEEK, bioactive glass, lawsone

---

**How to cite this article:** Ur Rehman MA, Bastan FE, Nawaz Q, Goldmann WH, Maqbool M, Virtanen SBoccaccini AR. 2018. Electrophoretic deposition of lawsone loaded bioactive glass (BG)/chitosan composite on polyetheretherketone (PEEK)/BG layers as antibacterial and bioactive coating. *J Biomed Mater Res Part A* 2018;106A:3111–3122.

---

## INTRODUCTION

There is an ever increasing need for developing antibacterial surfaces of implants that can combat the colonization of antibiotic resistant micro-organisms.<sup>1–5</sup> The local delivery of biologically active agents can reduce the risk of infections by providing high local concentrations in a controlled manner.<sup>4</sup>

In this context, herbal drugs have increasingly become the focus of biomedical research due to their wide range of biological effects.<sup>6,7</sup> Moreover, herbal medicines can be considered a healthy alternative to established drugs. The *Lawsonia inermis* (Henna) is a plant known as cosmetic agent, used for example to stain hair, skin and nails.<sup>8,9</sup> However, it is not only relevant to cosmetics; the phytochemical

constituents of *Lawsonia inermis* possess anti-inflammatory, antimicrobial, immune-stimulant, tumor inhibitory and wound healing potential along with low toxicity (the cytotoxic properties of henna and its derivatives have been reviewed<sup>9</sup>). The active component of henna is lawsone (2-hydroxy-1,4-naphthoquinone), which has been shown to exhibit antimicrobial properties.<sup>6,7,9</sup> Lawsone presents antibacterial activity; especially against gram positive bacteria. Moreover, lawsone possess antifungal effect and wound healing activity, which are prime requirements for biomedical applications in which lawsone can be combined with engineering biomaterials. In general, lawsone is active against gram positive bacteria, but inactive against gram

**Correspondence to:** A. R. Boccaccini; e-mail: aldo.boccaccini@ww.uni-erlangen.de  
Contract grant sponsor: Faculty development program (Institute of Space Technology, Islamabad, Pakistan)

negative bacteria.<sup>6,8</sup> The molecular structure of naphthoquinones has redox properties, which can cause antibacterial activity in various biological and oxidative processes. Naphthoquinones exhibit a wide spectrum of biological activity, yet, the antibacterial mechanism remains unclear.<sup>6-8,10</sup> These findings paved the way for the incorporation of lawsone as an antibacterial agent in composite coatings for potential orthopedic applications, that is, the main objective of the present research.

Drug delivery systems are important because they can maintain a given therapeutic level of a drug at the targeted site over a determined period of time, which is effective to reduce bacterial infections. Moreover, local drug delivery systems can also prevent the potential risk of cytotoxicity and accelerate the healing process at the defect site.<sup>11,12</sup>

PEEK is often employed as a mechanically robust biomaterial for orthopedic, trauma, and spinal implants.<sup>13,14</sup> PEEK consists of an aromatic backbone molecular chain, interconnected by ketone and ether functional groups.<sup>14-17</sup> PEEK is compatible with bioactive inorganic materials, including hydroxyapatite and bioactive glasses (BGs), which can be used either as a composite filler or as surface coating.<sup>13,18,19</sup> In addition, PEEK/BG composite layers can act as substrate to be further coated with biodegradable composite coatings loaded with antibiotics to provide improved surfaces for antiseptic bonding to tissues.<sup>20,21</sup>

Natural polymers are promising candidates for biomedical applications. Chitosan is a natural cationic polymer, which is derived from chitin through *N*-deacetylation. Chitosan is a biodegradable, biocompatible biopolymer for applications in drug delivery systems and tissue engineering, which can accelerate wound healing owing to its biocompatibility and antibacterial effects.<sup>22-24</sup> Electrophoretic deposition (EPD) is a widely adopted method for depositing inorganic particles, biopolymers and combination of both.<sup>25,26</sup> EPD harnesses the motion of charged particles or molecules in a liquid medium under the application of an electric field.<sup>25</sup> In addition to its economic advantages, being a low-cost process, EPD allows room temperature processing, which is beneficial for depositing biological molecules and drugs.<sup>23</sup> The coating thickness can be controlled easily through simple adjustment of deposition voltage, interelectrode distance and deposition time.<sup>27-29</sup> EPD of chitosan and bioactive glass was illustrated by Pishbin et al.,<sup>30</sup> in a study in which the EPD process was optimized by using a Taguchi Design of Experiment (DoE) approach and then chitosan/BG/gentamicin and chitosan/BG/Ag coatings were produced at the optimized parameters.<sup>2,4</sup> Chitosan-based bioactive coatings obtained by EPD present fairly homogenous microstructure, adequate in vitro bioactivity, enhanced cell attachment, good antibacterial activity and being suitable also for loading different drugs.<sup>2,4</sup> Moreover, Seuss, et al.<sup>31</sup> studied the alternating current (AC) EPD of chitosan/BG to inhibit the hydrolysis of water, which is not desired as it may cause bubble formation leading to uncontrolled porosity in the coatings. Recently, Heise et al.<sup>22,23</sup> deposited chitosan/BG and chitosan/BG/silica coatings on Dulbecco's Modified Eagle Medium (DMEM) pre-treated Mg alloy substrates. The

coatings showed good adhesion strength, improved corrosion resistance and in vitro bioactivity. Despite considerable research efforts on EPD of chitosan and its composite with inorganic particles, natural herbs have not been widely investigated for co-deposition by EPD along with chitosan/BG. Recently, we have deposited chitosan/silica glass nano particles/lawsone on PEEK/BG layer by EPD, which showed promising results.<sup>21</sup>

The focus of this research work was therefore to obtain antibacterial and bioactive coatings based on multilayer structured coatings based on combinations of polymers, that is, PEEK and chitosan. In this study, we employed EPD to develop chitosan/BG/lawsone composite coatings on a PEEK/BG composite layer previously deposited by EPD on stainless steel (SS). Multilayer coatings exhibited enhanced corrosion resistance at mild hydrophobicity. Moreover, preliminary in vitro bioactivity and antibacterial studies yielded promising results. To the best of the authors knowledge the combination of chitosan/BG/lawsone layers on PEEK/BG coatings has never previously been investigated to attain multifunctional bioactive and antibacterial coatings.

## EXPERIMENTAL PROCEDURE

### EPD of PEEK/BG

A 2 wt % PEEK powder (mean particle size of 10  $\mu\text{m}$ , 704XF Victrex<sup>TM</sup>) and 6.67 wt % bioactive glass (BG) powder of 2  $\mu\text{m}$  average particle size (Schott<sup>TM</sup>, Germany) with nominal 45S5 composition (45 SiO<sub>2</sub>-24.5 Na<sub>2</sub>O-24.5 CaO-6 P<sub>2</sub>O<sub>5</sub> (wt %))<sup>32</sup> were mixed in ethanol. About 13.32 wt % citric acid powder (monohydrate, VWR<sup>TM</sup> International) was added in the suspension to stabilize the BG and PEEK particles, following previous studies.<sup>33-35</sup> The addition of citric acid helps to charge the PEEK and BG particles negatively (zeta potential of the suspension was -10.2 mV<sup>35</sup>). 316 L SS foils (with a width of 1.5 cm and a thickness of 0.2 mm, cut to a length of 3 cm and cleaned with ethanol) were used as the deposition and counter electrodes (deposition area 225 mm<sup>2</sup>) for constant voltage EPD. An inter-electrode spacing of 0.5 cm, deposition voltage of 110 V and deposition time of 2 min were employed (following results of previous studies on EPD of PEEK/BG<sup>33-36</sup>). The coatings were sintered in a furnace (Nabertherm<sup>TM</sup> GmbH) at 400 °C for 30 min at a ramp rate of 2 °C min<sup>-1</sup>.

### EPD of chitosan/BG/lawsone

About 0.5 g L<sup>-1</sup> chitosan (medium molecular weight, 75-85% deacetylation degree, Sigma Aldrich<sup>TM</sup>) was dissolved in 20 Vol.% distilled water (ELGA DV 25 PURELAB option R7BP) and 1 Vol % acetic acid (VWR international) by magnetic stirring for 30 min. The 79 vol % ethanol (99-100%) was added to the chitosan dissolved solution to reduce the unsolicited hydrolysis of water during the EPD process, which may affect the homogeneity of the coatings, following the results of previous studies.<sup>4,23</sup> Afterwards, 0.5 g L<sup>-1</sup> bioactive glass powder and 0.5 g L<sup>-1</sup> lawsone (Sigma Aldrich<sup>TM</sup>, Germany) were added to the prepared chitosan solution. The stability of the suspension was determined by zeta-potential measurements using a zetasizer

(nano ZS equipment, Malvern Instruments™, UK). The suspension was stirred magnetically for 5 min and ultrasonicated for 1 h to ensure the dispersion of the BG particles. Initially, the EPD of chitosan/BG/lawsone was optimized on SS substrates. Finally, the optimized parameters were applied on PEEK/BG coated 316 L SS (as described in EPD of PEEK/BG section) substrates. The details of EPD parameters are shown in Table I.

### Characterization of the coatings

The surface morphology of the coatings was analyzed by field emission scanning electron microscope (FESEM, LEO 435VP, Carl Zeiss™ AG) at an energy of 10–15 kV. Samples were sputter-coated (Q150/S, Quorum Technologies™) with gold prior to FESEM analysis to prevent the effect of charging on the sample. Compositional analysis was performed qualitatively by: energy-dispersive x-ray spectroscopy (EDX) at 15 kV (LEO 435VP, Carl Zeiss™ AG) and Fourier Transformed Infrared spectroscopy (FTIR; Nicolet 6700, Thermo Scientific™) in transmittance mode for wavenumber values ranging from 4000 to 400  $\text{cm}^{-1}$ . To determine the relative mass ratio between polymer and ceramic contents in the coatings, thermogravimetric analyses (TGA 2950, TA Instruments) were performed.

Corrosion studies were carried out by immersing the coatings in Dulbecco's modified eagle medium (DMEM) at 37 °C and plotting the dynamic polarization curve at the scan rate of 3  $\text{mV s}^{-1}$ , in the potential range from  $E_{\text{corr}} - 500 \text{ mV}$  to  $E_{\text{corr}} + 500 \text{ mV}$  (IM6eX Xpot potentiostat, Zahner Elektrik GmbH). A three-electrode system, with Pt as a counter electrode, Ag/AgCl as a reference electrode and the substrate to be tested as working electrode, was used as a working electrode. The contact angle was measured (DSA30 Krüss GmbH, Germany) using deionized water droplets to evaluate the wettability of the coatings, since this property is essential for determining the initial protein attachment, which, in turn, is relevant for the intended biomedical applications in bone replacement devices. Roughness was measured by using a laser profilometer (UBM, ISC-2). A measurement length of 5–7 mm was used at a scan speed of 400 points per second. The roughness was calculated by the LMT Surface View UBM software.

To determine the acellular in vitro bioactivity of the coatings in terms of hydroxyapatite (HAp) formation, the Simulated Body Fluid (SBF) test, as proposed by Kokubo et al.,<sup>37</sup> was performed. The coated samples (15 mm × 15 mm × 0.2 mm) were immersed in 50 mL of SBF and were then incubated at 37 °C for 3, 7 and 14 days. At each time point samples were removed from SBF, rinsed with distilled water and left to dry in air. The formation of apatite like layer after incubation was examined with SEM/EDX, XRD (D8 Advance, Bruker™) and FTIR techniques.

The effect of lawsone in the coatings was investigated by drug release and antibacterial tests. To measure the release of lawsone from multilayer (ML) coatings the characteristic absorption peak for lawsone was measured, using a UV/VIS Spectrometer (Specord40 by Analytikjena) and analyzed by WinASPECT 2.5.8.0 software. The characteristic absorption peak of lawsone was determined at 455 nm. The drug release was measured by immersing ML coatings (15 × 15  $\text{mm}^2$ ) in 10 mL of phosphate buffered saline (PBS) and then incubated at 37 °C for 1 h to 180 days (in triplicate). At each time point (1 h, 2 h, 6 h, 1d, 3d, 5d, 1w, 1 m, 2 m, 3 m, 4 m, 5 m, and 6 m) 1 mL of the PBS was taken out for measurements and replaced with fresh PBS to maintain the physiological conditions. The cumulative release ( $m_c$ ) of lawsone (in  $\mu\text{g}$ ) was obtained by adding the mass of lawsone obtained at each time point. The percentage of cumulative drug release at each time point ( $\rho_x$ ) was calculated by using the following equation:

$$\rho_x = \frac{m_x}{m_t} \times 100$$

$m_x$  = mass of drug release at individual time points.

$m_t$  = cumulative mass of drug released in 180 days.

$\rho_x$  = percentage of cumulative drug release at each time point.

Agar disk diffusion tests were performed for chitosan/BG/lawsone coatings deposited on SS and on PEEK/BG layer. The PEEK/BG and chitosan/BG coatings deposited on SS were used as control samples. Prior to this study coatings were sterilized under UV light for 45 min. Agar plates were filled with 20 mL of agar and then 20  $\mu\text{L}$  of LB-media (Gram positive: *staphylococcus carnosus*) at an

**TABLE I. Summary for the Key Processing Parameters and Suspension Related Properties for EPD of Chitosan/BG/Lawsone Composite Coatings on PEEK/BG Layer**

Suspension Properties		EPD Process Parameters	
Chitosan type	Medium molecular weight with 75–85% deacetylation degree	Appl. voltage (V)	50
Chitosan conc. ( $\text{g L}^{-1}$ )	0.5	Deposition time (min.)	5
Bioactive glass type	45S5 bioactive glass (mean size: 2 $\mu\text{m}$ )	Inter-electrode distance (mm)	10
BG conc. ( $\text{g L}^{-1}$ )	0.5	Substrate; counter electrode	PEEK/BG; 316 L SS
		Coating thickness	110 microns (Multilayer coatings)
Lawsone con. ( $\text{g L}^{-1}$ )	0.5		
Solvent composition	Acetic acid (1 Vol. %) – Ethanol (79 Vol. %) – Water (20 Vol. %)		
Zeta pot. and pH	+40 mV and pH 4.2		

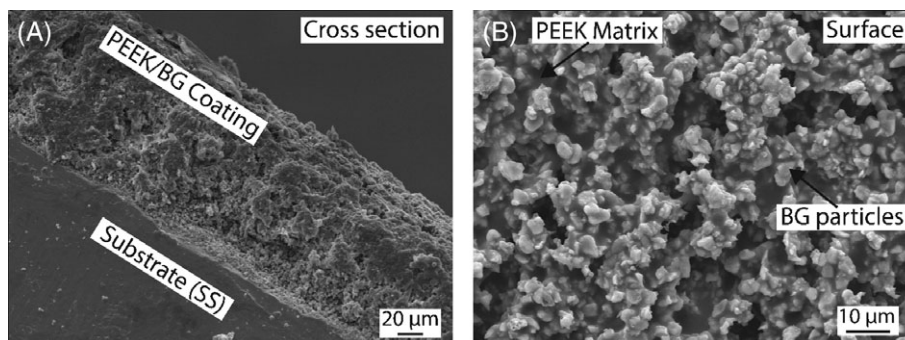


**FIGURE 1.** SEM images of PEEK/BG composite coatings produced at an applied electric field of  $22 \text{ kV m}^{-1}$ , 2 min, and sintered at  $400^\circ\text{C}$ ; (A) cross-section, (B) top surface.

optical density of 0.015 ( $\text{OD}_{600}$ ) were spread homogeneously on the agar plates. The samples were placed on the prepared agar plates, which were kept in the incubator at  $37^\circ\text{C}$  for 24 h. After incubation, the inhibition zones were measured by using 'ImageJ' analysis (each test was performed in triplicate).

## RESULTS

### PEEK/BG composite coatings on 316 L SS

Figure 1 (A,B) shows SEM micrographs of PEEK/BG composite coating obtained at  $22 \text{ kV m}^{-1}$ , 2 min, and sintered at  $400^\circ\text{C}$  in two magnifications. Figure 1(B) indicates that the sintered PEEK /BG coating was fairly homogenous exhibiting a porous microstructure. Moreover, the coatings have relatively high particle density and a uniform coating thickness of  $80\text{--}90 \mu\text{m}$  [Fig. 1(A)].

### EPD of chitosan/ BG/lawsone

**Suspension stability in terms of zeta potential.** The stability of the suspension (chitosan/BG/lawsone) was assessed in terms of zeta potential, which was  $+40 \pm 5 \text{ mV}$  at pH 4.2, a value which is in accordance with previous studies on chitosan/BG.<sup>2,4,23</sup> The 'positive' charge indicates that the particles/molecules will migrate to the cathode during EPD. The addition of lawsone in the suspension did not have a detrimental effect on the charge and stability of the suspensions (lawsone alone when dispersed in ethanol and water

showed a zeta potential of  $+55 \pm 5 \text{ mV}$  at pH 4.2), which suggests that lawsone can be codeposited along with chitosan and BG.

### EPD process of chitosan/BG/lawsone on 316 L SS.

The EPD process for chitosan/BG/lawsone was optimized on 316 L SS substrates by Taguchi Design of Experiment (DoE) approach (data not shown, available on request). Figure 2(A) illustrates the effect of deposition voltage and time on the resulting current density during EPD. The current density at each applied voltage shows almost the same trend; initially there is a steep decrease in current density and later the plot becomes nearly a straight line.<sup>28</sup> The EPD parameters are often optimized in terms of deposition yield.<sup>25,28</sup> Figure 2 (B) shows the effect of applied voltage on deposition yield at 5 min of deposition time. With an increase in deposition voltage particles having low electrophoretic mobility can also be deposited on the substrate along with BG particles, which leads to the increase in deposition yield. Thus, results showed that at a constant deposition time (5 min), more particles were able to move and coagulate at the substrate.<sup>28</sup>

The optimized EPD parameters were: (i) applied voltage of 30 V, (ii) deposition time of 5 min, and (iii) interelectrode distance of 1 cm. Fairly homogenous coatings were obtained by using such optimized parameters, as shown in Figure 3 (A). The BG particles were dispersed homogeneously in the chitosan matrix. The SEM image of the cross section [Fig. 3

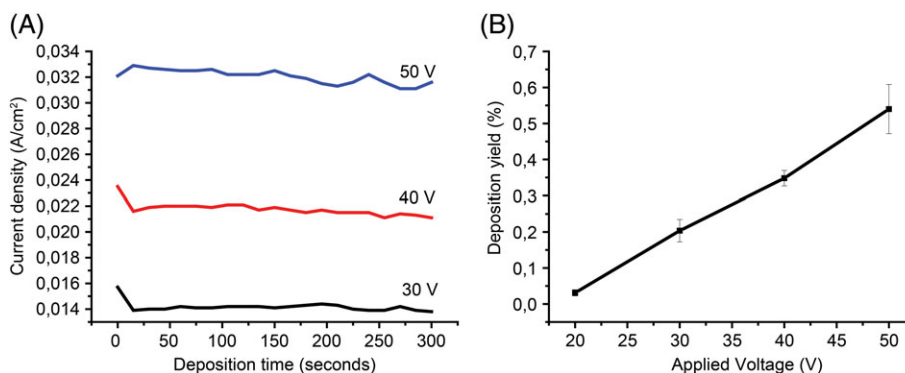


**FIGURE 2.** EPD of chitosan/ BG/ lawsone: (A) relationship among different EPD parameters (applied potential, deposition time and the resulting current density) during the EPD process, (B) relationship between applied voltage and resulting deposition yield during the EPD process at 5 min of deposition time.

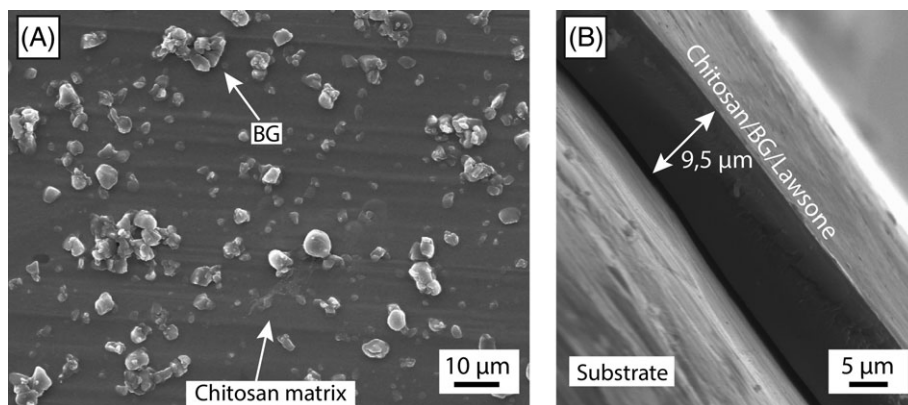


**FIGURE 3.** SEM images of chitosan/BG/lawsone coatings developed on 316 L SS via EPD at 30 V and 5 min of deposition time: (A) top surface, (B) cross section.

(B)] shows that coatings have uniform thickness of 8–10 µm and excellent film forming ability.

#### EPD of chitosan/BG/lawsone on PEEK/BG layer

Once the EPD process was optimized for chitosan/BG/lawsone on stainless steel, the same parameters were investigated for the deposition on the PEEK/BG layers to develop multilayer (ML) coatings. However, the insulation effect of PEEK/BG layer reduced the current density due to which deposition voltage of 50 V was employed.

**Morphological analysis.** SEM images of the coating surface show the successful deposition of chitosan/BG/lawsone on PEEK/BG layer [Fig. 4(A)]. The chitosan/BG/lawsone layer covers the underlying PEEK/BG layer by filling the pores in most instances. High magnification images showed that chitosan may have formed a nanoscale film on PEEK/BG layer, as indicated by the arrows in Figure 4(B,C).

**Compositional analysis.** Figure 5(A) shows the FTIR spectrum of chitosan/BG/lawsone coating on SS substrate and on PEEK/BG layer. FTIR spectra of chitosan/BG/lawsone coatings on SS and on PEEK/BG layer showed the characteristic peaks of chitosan and BG. Figure 5(B) illustrates the thermogravimetric analysis (TGA) of the PEEK/BG coatings sintered at 400 °C and chitosan/BG/lawsone coatings on

PEEK/BG layer. TGA results were used to determine the relative contents of organic and inorganic materials in the composite system.

**Wetting behavior.** The static water contact angle measurements are used to evaluate the wettability of coatings (Fig. 6). PEEK/BG coatings when sintered at 400° showed a contact angle of 100° ( $\pm 7\%$ ) (mildly hydrophobic). On the other hand, chitosan/BG/lawsone coatings on PEEK/BG layer showed a contact angle of 45° ( $\pm 7\%$ ).

**Roughness measurements.** Surface roughness is one of the key parameters affecting cell attachment and proliferation. PEEK/BG composite coatings presented a mean roughness ( $R_a$ ) of  $2.2 \pm 0.1$  µm and maximum roughness ( $R_{max}$ ) of  $16 \pm 1$  µm (Table II). However, the multilayer coatings showed a  $R_a$  value of  $1.3 \pm 0.2$  and a  $R_{max}$  value of  $7 \pm 2$ .

**Corrosion studies.** Figure 7 shows the potentiodynamic polarization curves for the bare SS, PEEK/BG, and ML coatings in the applied potential range of  $E \pm 500$  mV and at a scan rate of  $3 \text{ mV sec}^{-1}$ .<sup>38</sup> The bare 316 L SS shows passivation behavior, but the corrosion current density is higher than for both coated samples, indicating that the coatings offer corrosion protection.

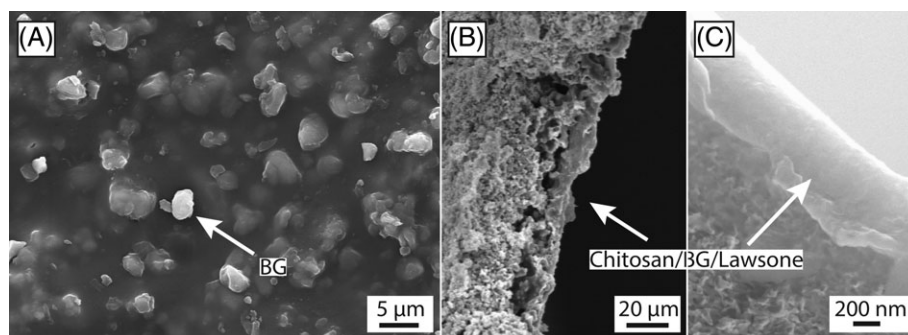


**FIGURE 4.** SEM images of chitosan/BG/lawsone coatings developed on PEEK/BG layer via EPD at 50 V and 5 min of deposition time: (A) top surface image, (B) image of the cross-section, (C) high magnification image of the cross-section.

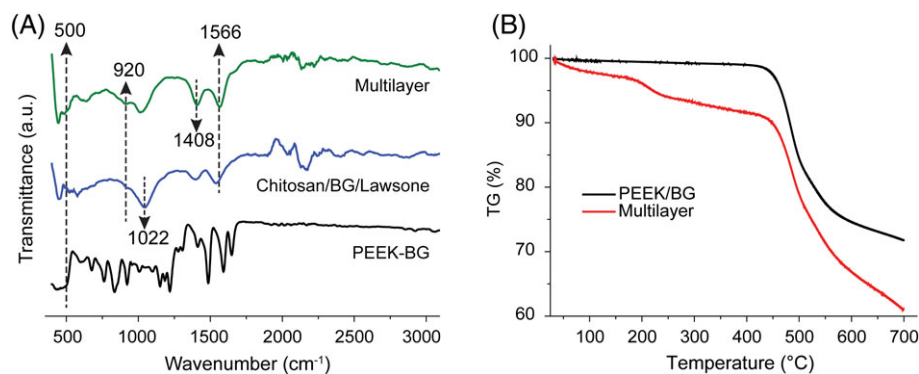


**FIGURE 5.** (A) FTIR spectrum of PEEK/BG, chitosan/BG/lawsone, and multilayer coatings, (B) thermogravimetric analysis of PEEK/BG coatings sintered at 400 °C and multilayer coatings.

**In vitro bioactivity.** SEM micrographs show the change in the morphology of the coating surface after immersion in SBF, characterized by the formation of pores and a nano-structured apatite layer (Fig. 8).

EDX analysis shows the increase in the relative intensity of P and Ca peaks and the decrease in intensity of Si peaks (EDX spectrum in Fig. 8), in comparison to the coatings before immersion in SBF. The XRD analysis confirmed the formation of new phases after immersion in SBF, as shown in Figure 9(A). Moreover, FTIR analysis indicated the formation of new bonds upon immersion of ML coatings in SBF, as shown in Figure 9(B).

**Drug release study.** The drug release curve can be divided into three main regions (Fig. 10). Region I corresponds to the initial release during the first day, in which almost 12% of the drug was released. In region II, drug was released at a relatively higher rate and almost 88% of the drug was released. In region III, the lawsone was released very slowly and the remaining amount of lawsone (12%) was released after 180 days of incubation (Region III, Fig. 10).

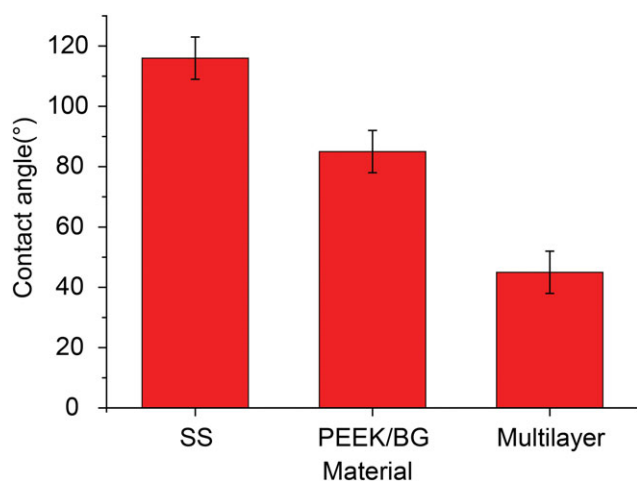


**FIGURE 6.** Wetting behavior of SS, PEEK/BG coatings sintered at 400 °C and multilayer coatings (The data indicate mean  $\pm$  standard deviation for five coatings).

**Antibacterial studies.** The antibacterial activity of ML coatings and chitosan/BG/lawsone on SS was determined by the formation of inhibition zone on agar medium by the direct contact method with *S. carnosus* (Fig. 11). The coatings were placed on bacteria inoculated plates, whereas PEEK/BG and chitosan/BG coatings were used as control samples. The control samples did not show antibacterial activity. However, chitosan/BG/lawsone coatings deposited on SS and ML coatings developed inhibition halo against *S. carnosus*. The zone of inhibition halo was measured by using “ImageJ” analysis. Chitosan/BG/lawsone coatings on 316 L SS developed larger inhibition halo zone ( $10 \pm 1$  mm) than the ML ( $4 \pm 1$  mm) coatings.

## DISCUSSION

In this work, EPD was successfully used to deposit multi-structured coatings on 316 L SS substrates. Firstly, PEEK/BG composite coatings (Fig. 1) were deposited via EPD on 316 L SS substrates. The details about the effect of deposition kinetics and mechanism on the morphology and thickness of PEEK/BG coatings have been discussed in the literature.<sup>35</sup>

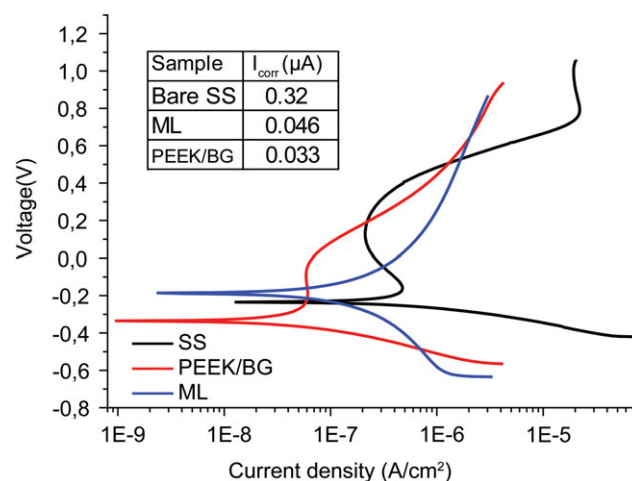


**FIGURE 7.** Polarization curves obtained by using DMEM at 37 °C for bare SS, PEEK/BG coatings sintered at 400 °C and multilayer coatings.

**TABLE II. Roughness Measurements for PEEK/BG Coatings Sintered at 400 °C and for Multilayer Coatings**

Substrate	Mean Roughness ( $R_a$ ) $\mu\text{m}$	Maximum Roughness ( $R_{\text{max}}$ ) $\mu\text{m}$
Chitosan/BG/lawsone on PEEK/BG layer (ML)	$1.3 \pm 0.2$	$7 \pm 2 \mu\text{m}$
PEEK/BG sintered at 400 °C	$2.2 \pm 0.1$	$16 \pm 1 \mu\text{m}$

Secondly, chitosan/BG/lawsone coatings (Fig. 4) were deposited on PEEK/BG layers (previously deposited by EPD).

### EPD of chitosan/BG/lawsone

**Suspension stability.** To deposit chitosan/BG/lawsone coatings a stable suspension with zeta potential of  $+40 \pm 5 \text{ mV}$  at pH 4.2 was prepared. The relatively high value of zeta potential indicates the stability of the suspension, which is important to obtain uniform coatings by EPD. The EPD mechanism of chitosan/BG deposits has been explained by Pishbin et al.<sup>4</sup> Uncharged chitosan is insoluble in water and organic solvents. However, protonated chitosan dissolves in water-ethanol-acetic acid mixtures at low pH ( $\sim\text{pH} < 5$ ).<sup>4,31</sup> During the application of an electric field (EPD process), positively charged chitosan molecules move towards the cathode, lose their charge and form an insoluble deposit at the cathode.<sup>39,40</sup> Moreover, BG and lawsone are positively charged under acidic pH, hence they are expected to move towards the cathode and deposit by coagulation. The electrophoretic mobility of BG particles is much higher than that of chitosan and lawsone. Therefore, at low concentration of BG codeposition of chitosan/BG/lawsone is expected. However, higher

concentrations of BG will lead to a substantial decrease in the electrophoretic mobility of chitosan and lawsone (due to the increase in pH and conductivity). These findings formed the basis for choosing equal concentration of chitosan, BG and lawsone in this study.

**EPD of chitosan/BG/lawsone on 316 L SS.** The EPD process of chitosan/BG/lawsone was first optimized on 316 L SS by applying a Taguchi Design of Experiment approach (data not shown here). SEM images of the top surface of chitosan/BG/lawsone coating on 316 L SS showed a uniform distribution of BG particles in the chitosan matrix [Fig. 3(A)]. Moreover, lawsone dissolved completely during the suspension preparation, which may have contributed to the formation of films [Fig. 3(B)]. Moreover, SEM images of the cross section show that chitosan/BG/lawsone coating developed a uniform thickness (8–10  $\mu\text{m}$ ). However, slight variations in the coating thicknesses and homogeneity have been observed among different researchers, as well as in the current study, which is possibly due to the difference in particle size and concentration of BG along with the variations in EPD parameters.<sup>4,23,30,41,42</sup>

**EPD of chitosan/BG/lawsone on PEEK/BG layer.** After optimizing the EPD process of chitosan/BG/lawsone on 316 L SS, similar EPD conditions were applied to obtain chitosan/BG/lawsone coatings on PEEK/BG layers. SEM images of the top surface of the multilayer (ML) coatings confirmed the deposition of chitosan/BG/lawsone on top of the PEEK/BG layer. However, SEM did not show a clear interface between the two layers, that is, PEEK/BG and chitosan/BG/lawsone, possibly due to the fact that the maximum roughness ( $R_{\text{max}}$ )

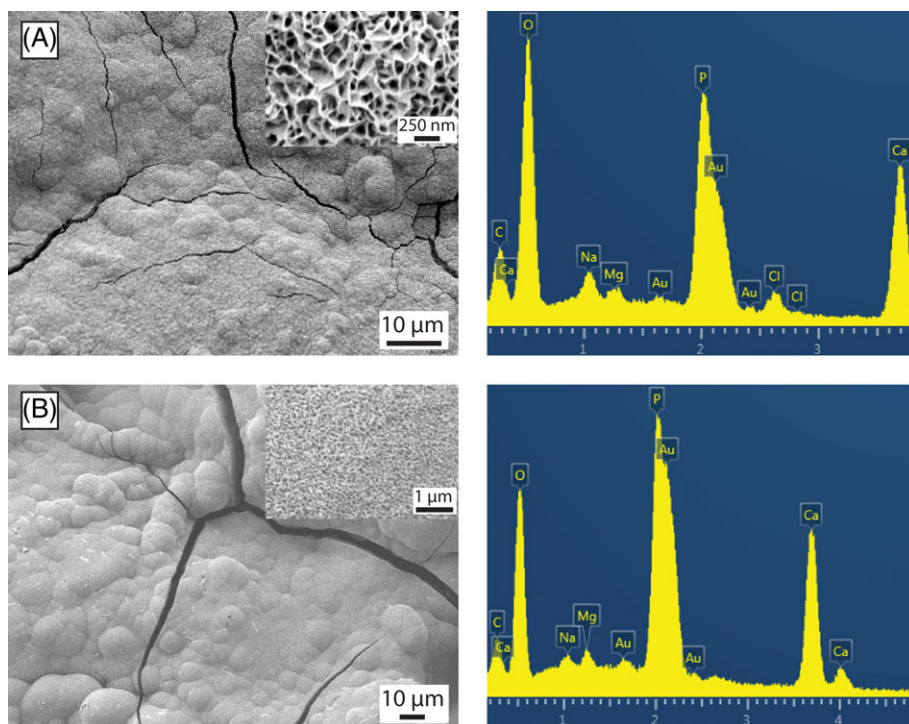


**FIGURE 8.** SEM images and corresponding EDX spectra of the surface of multilayer coatings after treatment in SBF for (A) 3 days and (B) 7 days.

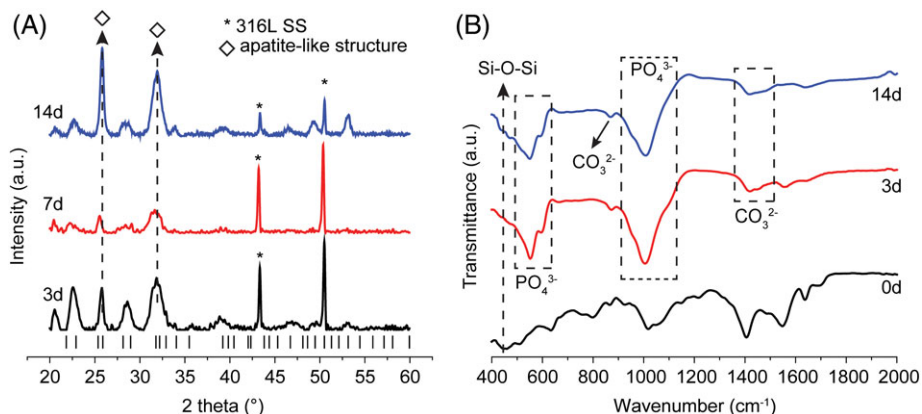


**FIGURE 9.** (A) XRD patterns of multilayer coatings after treatment in SBF for 3, 7, and 14 days, (B) FTIR spectra of multilayer coatings before and after treatment in SBF for 3 and 14 days.

of the sintered PEEK/BG layer was  $16 \pm 1 \mu\text{m}$ , and the coating thickness of the chitosan/BG/lawsone layer was in the range of 8–10  $\mu\text{m}$ , due to which the top layer was able to fill the pores in the PEEK/BG layer and no clear interface was formed, as shown in Figure 4(B,C). However, it was observed in high magnification images that chitosan may have formed a nanoscale film on the PEEK/BG layer, as indicated by the arrows in Figure 4(B,C).

### Compositional analysis

FTIR analysis [Fig. 5(A)] confirmed the presence of chitosan/BG/PEEK in the multilayer coatings and chitosan/BG in the chitosan/BG/lawsone coatings. The characteristic peaks of BG were determined in ML and PEEK/BG coatings at  $460\text{--}500 \text{ cm}^{-1}$  (bending vibration of Si-O-Si) and at  $920\text{--}1030 \text{ cm}^{-1}$  (stretching vibration of network modifiers in the glass structure<sup>4</sup>). The characteristic peaks of chitosan were determined in ML and chitosan/BG/lawsone coatings such as stretching vibration of the C–O bond in chitosan at  $1080 \text{ cm}^{-1}$ .<sup>41,42</sup> The broad band around  $1022 \text{ cm}^{-1}$  may have appeared due to the overlapping of the C–O bond in

chitosan and the network modifiers in the glass structure.<sup>2</sup> Moreover, the band at about  $1408 \text{ cm}^{-1}$  is assigned to the asymmetrical bending in C–H and the band around  $1570 \text{ cm}^{-1}$  is ascribed to the N–H bonding vibration of chitosan.<sup>43,44</sup> FTIR spectra of chitosan/BG/lawsone and ML coatings exhibit bands at  $2030 \text{ cm}^{-1}$  and  $2160 \text{ cm}^{-1}$ , which are assigned to the aromatic ring and thiocyanate group of lawsone, respectively.<sup>45</sup> However, the effect of lawsone was not clearly observed in the FTIR spectra of ML coatings, possibly due to the hydrogen bonding between hydroxyl groups of lawsone and chitosan, which may have caused the overlapping of chitosan and lawsone bands.

After acquiring conclusive evidence about the presence of chitosan/BG/PEEK in the multilayer coatings and of

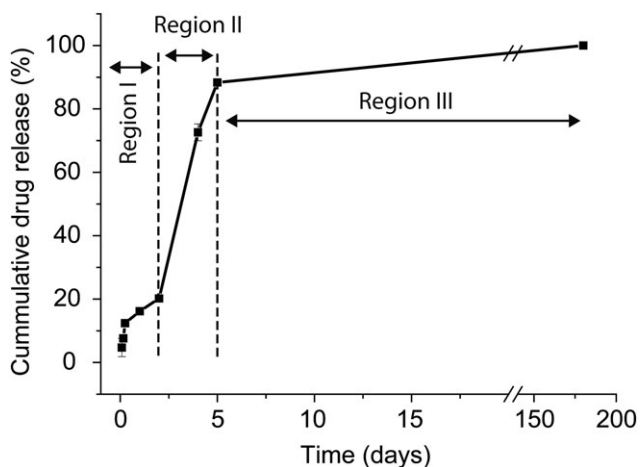


**FIGURE 10.** Cumulative release of lawsone in PBS from EPD coatings of chitosan/BG/lawsone (The data indicate mean  $\pm$  standard deviation for three individual experiments).

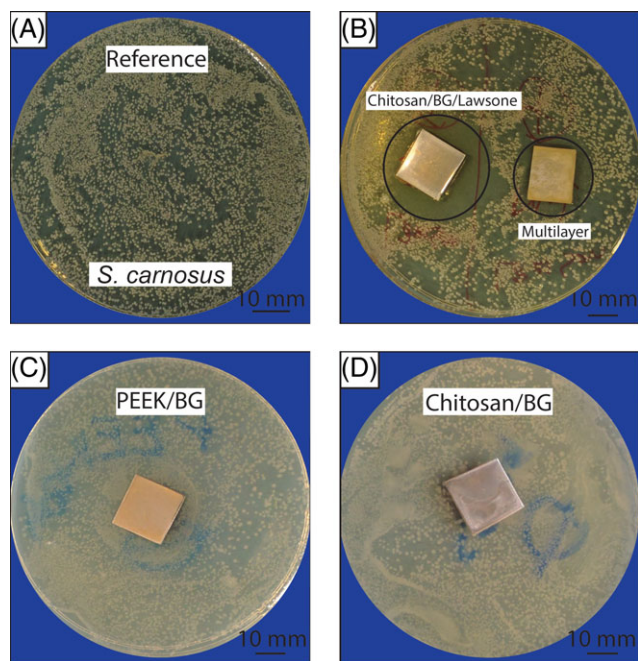


**FIGURE 11.** Inhibition halo test with *S. carnosus* for (A) reference sample, (B) chitosan/BG/lawsone on SS and multilayer coatings, (C) PEEK/BG (control sample), and (D) chitosan/BG (control sample).

chitosan/BG in chitosan/BG/lawsone coatings, TGA was performed to determine the composition of the coatings quantitatively [Fig. 5(B)]. The sintered PEEK/BG coating showed a plateau up to  $\sim 425$  °C, which indicates the thermal stability of the PEEK matrix. PEEK starts to evaporate above this temperature, and is released almost completely at 700 °C. The remaining mass may be considered as the relative content of BG (wt. %) in the composite system.<sup>46</sup> It was inferred from the TGA measurement that the PEEK/BG weight ratio was around 30:70 (PEEK:BG), which is a suitable composition to achieve in vitro bioactivity and adhesion strength (data shown in our previous study<sup>35</sup>).

TGA of chitosan showed a minor weight loss up to 100 °C, which can be due to the release of adsorbed water, and then chitosan burns out above this temperature.<sup>47</sup> In this study two more regions in the TGA curve of the multilayer system were recognized. The weight loss up to about 200 °C was due to the release of adsorbed water. The liberation of adsorbed water may be extended over the temperature range due to the deposition of the chitosan/BG/lawsone coating in the porous PEEK/BG layer. Subsequently, the slow mass changes up to  $\sim 600$  °C can correspond to the burning out of chitosan; afterwards, the TGA curve becomes similar to the TGA curve of PEEK/BG layer.

The ML coating showed a weight loss of  $\sim 22\%$ ,  $\sim 34\%$ , and  $\sim 39\%$  at 500 °C, 600 °C and 700 °C, respectively. The weight loss in ML coatings in the range of 500 °C – 700 °C is attributed to the degradation of PEEK and chitosan. PEEK/BG coatings showed a weight loss  $\sim 15\%$ ,  $\sim 25\%$ , and  $\sim 30\%$  at 500 °C, 600 °C and 700 °C, respectively. This weight loss in PEEK/BG coatings in the range of 500 °C – 700 °C is attributed to the degradation of PEEK. The difference in weight loss between two coatings (PEEK/BG and ML coatings) in the range of 500 °C – 600 °C is mainly due to the difference in composition of the two coatings. ML coatings contained two polymers, that is, chitosan and PEEK, due to which the weight loss in ML coating was significantly higher (range of 500 °C – 600 °C) in comparison to the PEEK/BG coatings. It was concluded from the TGA analysis that the multilayer system contains 8–10 wt % of chitosan/lawsone and 90–92 wt % of PEEK/BG.

### Wetting behavior

The contact angle of 55° is considered suitable for improved cell attachment and spreading.<sup>48</sup> Multilayer coatings exhibited contact angle of 45° (Fig. 6), which is the result of the combination of hydrophobic side chains of chitosan and hydrophilic Si–OH bonds of BG.<sup>23</sup> The distribution of BG particles on the top of the coating may be responsible for the decrease in the contact angle of multilayer coatings. The contact angle (45°) is in a range suitable for orthopedic applications.<sup>23</sup> Similar values for the contact angle of chitosan/BG coatings have been reported in the literature.<sup>23</sup>

### Roughness measurements

Multilayer coatings showed a decrease in the roughness values ( $R_{\max}$ ,  $R_a$ ) in comparison to PEEK/BG coatings, which indicates that chitosan/BG/lawsone layer fills the pores and

decreases the roughness of the PEEK/BG layer. Moreover, the filling of the pores with chitosan/BG/lawsone could also be useful in sustaining the release of the drug for longer periods of time. The mean roughness of ML coatings is still above 1  $\mu\text{m}$  (Table II), which can be considered adequate for supporting cell attachment and spreading.<sup>49</sup>

### Corrosion studies

PEEK/BG and multilayer coatings showed the corrosion protection behavior as determined from the polarization curve (Fig. 7). ML coated samples show a continuous increase of the current densities upon anodic polarization, indicating coating dissolution. Noteworthy is the strong decrease of the cathodic current densities for the coated samples. A Tafel extrapolation was carried out leading to corrosion current densities ( $i_{\text{corr}}$ ) of 0.32  $\mu\text{A cm}^{-2}$ , 0.033  $\mu\text{A cm}^{-2}$ , and 0.046  $\mu\text{A cm}^{-2}$  for bare SS, PEEK/BG, and multilayer coatings, respectively. The current density for ML coatings was slightly higher than that of the PEEK/BG composite coatings. This effect may occur due to the accelerated degradation of chitosan in DMEM under varying potential. However, statistically, the difference in  $I_{\text{corr}}$  values of ML and PEEK/BG coatings is negligible. The PEEK/BG coatings show a good corrosion protection effect, as the sintering process leads to the formation of a biostable film of PEEK reinforced with BG particles that effectively acts as a barrier on the metallic substrate.

### In vitro bioactivity

SEM images show that plate-like hydroxyapatite completely covered the surface of ML coating after 3 days of immersion in SBF [Fig. 8(A)]. The plate-like structure indicates the formation of a calcium enriched apatite layer.<sup>2,4,50</sup> Considering that the iso-electric point (IEP) of the PEEK/BG layer occurs at a pH lower than of the SBF (7.40); the PEEK/BG coatings likely exhibit negative charge in SBF and attract more positive  $\text{Ca}^{2+}$  ions. This fact may be responsible for a calcium dominated “plate-like” form of apatite. The inset micrographs in Figure 8(A,B) revealed a reduced porosity with increasing immersion time, from 3 to 7 days, which could be associated to the densification of the apatite-like layer. EDX analysis showed the increase in intensity of Ca and P peaks, which corresponds to the formation of the new calcium phosphate layer on the coatings.<sup>31</sup>

XRD analysis showed the presence of new diffraction peaks at  $2\theta = 25.8^\circ$  and  $31.6^\circ$  [Fig. 9(A)], which can be attributed to hydroxyapatite.<sup>4</sup> The relative intensity and sharpness of peaks increased with the increase in incubation time, which suggests the formation of higher proportion of HAP after 14 days.<sup>31</sup>

FTIR spectra of ML coatings after immersion in SBF [Fig. 9(B)] exhibited a reduction in intensity of the peaks related to BG (Si–O–Si at  $459\text{ cm}^{-1}$ )<sup>2</sup> and amide-I peaks of chitosan after 3 days. However, amide-II peaks ( $1558\text{ cm}^{-1}$  and  $1406\text{ cm}^{-1}$ )<sup>4</sup> completely vanished after 3 days of immersion, which indicates the degradation of chitosan. The formation of new phosphate peaks ( $564$ ,  $605$ ,  $963$  and  $1030\text{ cm}^{-1}$ <sup>2,4,51</sup>) and carbonate peaks ( $868\text{ cm}^{-1}$  and  $1418\text{ cm}^{-1}$ )<sup>2,4</sup>

indicated the formation of carbonated hydroxyapatite. The relative reduction in intensity of the peaks corresponding to BG ( $461\text{ cm}^{-1}$ ,  $650\text{ cm}^{-1}$  and  $902\text{ cm}^{-1}$ )<sup>51</sup> after 1 day of immersion in SBF indicates the start of the dissolution of BG through the release of  $\text{Ca}^{+2}$  and  $\text{Na}^{+}$  ions in critical concentrations.<sup>32,51</sup> Indeed the formation of carbonated HAP is the desired effect of adding BG to the coatings as it will promote the bone binding ability of the coatings.<sup>32,52</sup>

### Drug release study

In the drug release curve (Fig. 10) region I corresponds to the initial release of lawsone during the first day, in which almost 12% of the drug was released, which is mainly due to the diffusion of the molecules from the surface and smaller pores in the coatings.<sup>3,53</sup> After 1 day of immersion in phosphate buffer saline (PBS), chitosan matrix may start to degrade, which allows a higher drug release rate. Therefore, it can be concluded that during the first day lawsone is mainly released due to diffusion.<sup>3,54</sup> It was observed that after 1 day of incubation lawsone was released slowly compared to the first 24 h of incubation. The reason is likely that diffusion of the drug molecules depends on their concentration in the coating.<sup>3,54</sup> In the present study, lawsone was released in a burst manner from the top surface of the coatings during the first 24 h, thus the available concentration of lawsone on the coating surface was reduced after 24 h leading to a strong decrease in the release kinetics. However, after 3 days the combination of degradation and diffusion speeds up the drug release kinetics, and almost 88% of the drug was released during first 5 days (region II, Fig. 10).<sup>55</sup> Moreover, FTIR spectra after 3 days immersion in SBF also confirmed the degradation of chitosan (same effect has also been reported in the literature<sup>4</sup>).

In region III, the drug was released very slowly, which could be due to the fact that the chitosan matrix has degraded completely, but some amount of the drug may have remained in the deeper pores of the PEEK/BG layer. The higher roughness of the PEEK/BG layer facilitates the sustained release of lawsone over 6 months, as shown in Figure 10. Regarding region III, it is worth mentioning that drug release was above the minimum inhibitory concentration ( $\text{MIC} = 256\text{ }\mu\text{g mL}^{-1}$ ) after 120 days, which can lead to bacterial effect at the implant site even after 4 months.<sup>56</sup>

### Antibacterial studies

Chitosan/BG/lawsone coatings deposited on SS and ML coatings showed an antibacterial effect against *S. carnosus*. Chitosan/BG/lawsone coatings on 316 L SS showed a stronger antibacterial effect in comparison to the ML coatings. The reason could be that the ML structure decreases the release of lawsone due to the higher surface roughness of PEEK/BG layer, eventually forming a smaller halo after 1 day of incubation.<sup>3</sup> However, the application of chitosan/BG/lawsone on SS developed a larger inhibition halo due to the low surface roughness of 316 L SS (mean surface roughness of SS:  $0.2\text{ }\mu\text{m}$ ). This might be responsible for the higher release of lawsone than in ML coatings.<sup>3,4</sup> We concluded that ML coatings may be considered a preferred approach in achieving

the controlled release of lawsone over longer periods (e.g., 180 days) maintaining a long-term antibacterial effect ( $\text{MIC}$  was maintained up to 120 days<sup>56</sup>). A similar sort of multilayer strategy was proposed by Pishbin et al.<sup>4</sup> using electrophoretically deposited chitosan-based coatings, in order to achieve coatings with a sustained drug release.

The bactericidal property of lawsone is associated with the molecular structure of naphthoquinones, which impart redox properties thus inducing antibacterial activity in various biological and oxidative processes.<sup>6–10,56</sup> Although naphthoquinones exhibit a wide spectrum of biological activities, the actual mechanism of antibacterial effect remains unclear<sup>6,9</sup>, particularly when the herbal drug is combined with polymer coatings.

### CONCLUSIONS

PEEK/BG composite coatings deposited on 316 L stainless steel (SS) provided an effective substrate for the deposition of chitosan/BG/lawsone composite coatings by EPD. SEM and FTIR analyses showed the successful deposition of chitosan/BG on PEEK/BG layer. Moreover, the release of lawsone from ML coatings was confirmed by UV/VIS analyses. Chitosan/BG/lawsone coatings fill the pores in the PEEK/BG layer to some extent, thus reducing the overall roughness of the multilayer structure. Multilayer coatings show improved corrosion resistance in comparison to uncoated 316 L SS. Moreover, the multilayer coatings showed convenient wetting angle relevant for protein attachment. Chitosan/BG/lawsone coatings did not affect the initial *in vitro* bioactivity of the PEEK/BG layer but supported the formation of an apatite-like layer when immersed in SBF. Multilayer coatings showed a sustained drug release of lawsone for up to 6 months and exhibited antibacterial activity against *S. carnosus*. This research will contribute to consider PEEK-based bioactive coatings incorporating BG and herbal bioactive components in future *in vivo* investigations and eventually in clinical applications. Future work will focus on cell culture studies to track potential cytotoxic effects due to the release of lawsone. However, the multilayer structure is expected to provide controlled release of lawsone, to avoid cytotoxic effects and to provide long term antibacterial protection, despite the rapid degradation of chitosan.

### ACKNOWLEDGMENTS

The authors thank Barbara Myszkla for XRD analysis and Bilal Haider for performing TGA analysis. The results presented in this paper are part of the doctoral thesis submitted by Muhammad Atiq Ur Rehman to the University of Erlangen-Nuremberg.

### REFERENCES

1. Braem A, De Brucker K, Delattin N, Killian MS, Roeffaers MJB, Yoshioka T, Hayakawa S, Schmuki P, Cammue BPA, Virtanen S, Thevissen K, Neirinck B. Alternating current electrophoretic deposition for the immobilization of antimicrobial agents on titanium implant surfaces. *ACS Appl Mater Interfaces*. 2017;9:8533–8546.
2. Pishbin F, Mourinho V, Gilchrist JB, McComb DW, Kreppel S, Salih V, Ryan MP, Boccaccini AR. Single-step electrochemical deposition of antimicrobial orthopaedic coatings based on a bioactive

- glass/chitosan/nano-silver composite system. *Acta Biomater* 2013;9:7469–7479.
3. Simchi A, Tamjid E, Pishbin F, Boccaccini AR. Recent progress in inorganic and composite coatings with bactericidal capability for orthopaedic applications. *Nanomed Nanotechnol Biol Med* 2011;7:22–39.
  4. Pishbin F, Mouriño V, Flor S, Kreppel S, Salih V, Ryan MP, Boccaccini AR. Electrophoretic deposition of gentamicin-loaded bioactive glass/chitosan composite coatings for orthopaedic implants. *ACS Appl Mater Interfaces* 2014;6:8796–8806.
  5. Ferraris M, Balagna C, Perero S, Miola M, Ferraris S, Bairo F, Battiato A, Manfredotti C, Vittone E, Vern E. Silver nanocluster/silica composite coatings obtained by sputtering for antibacterial applications. *Mater Sci Eng* 2012;40:6.
  6. Gozubuyuk GS, Aktas E, Yigit N. An ancient plant *Lawsonia inermis* (henna): Determination of in vitro antifungal activity against dermatophyte species. *J Med Mycol* 2014;24:313–318.
  7. Sahar Traor M, Aliou Bald M, Camara AS, Sadou Bald E, Dian S, Telly Diallo MS, Keita A, Cos P, Maes L, Pieters L, Mamadou Bald A. The malaria co-infection challenge: An investigation into the antimicrobial activity of selected Guinean medicinal plants. *J Ethnopharmacol* 2015;174:576–581.
  8. Bastan FE, Ur Rehman MA, Avcu YY, Avcu E, Üstel F, Boccaccini AR. Chemopreventive action of *Lawsonia inermis* Leaf Extract on DMBA-induced skin papilloma and B16F10 melanoma tumour. *Pharmacol Online* 2009;1249:1243–1249.
  9. Babu P, Subhasree R. Antimicrobial activities of *Lawsonia inermis*—a review. *Acad J Plant Sci [Internet]* 2009;2:231–232.
  10. Kapadia GJ, Rao GS, Sridhar R, Ichiishi E, Takasaki M, Suzuki N, Konoshima T, Iida A, Tokuda H. Chemoprevention of skin cancer: Effect of *Lawsonia inermis* L. (Henna) leaf powder and its pigment artifact, lawsone in the Epstein-Barr virus early antigen activation assay and in two-stage mouse skin carcinogenesis models. *Anticancer Agents Med Chem* 2013;13:1500–1507.
  11. Mouriño V, Boccaccini AR. Bone tissue engineering therapeutics: Controlled drug delivery in three-dimensional scaffolds. *J R Soc Interface* 2010;7:209–227.
  12. Vallet-Regí M, Balas F, Arcos D. Mesoporous materials for drug delivery. *Angew Chem Int Ed* 2007;46:7548–7558.
  13. Ma R, Tang T. Current strategies to improve the bioactivity of PEEK. *Int J Mol Sci* 2014;15:5426–5445.
  14. Kurtz SM, Devine JN. PEEK biomaterials in trauma, orthopedic, and spinal implants. *Biomaterials*. 2007;28:4845–4869.
  15. Torres Y, Romero C, Qiang C, Pérez G, Rodríguez-Ortiz JA, Pavón JJ, Álvarez L, Arévalo C, Boccaccini AR. Electrophoretic deposition of PEEK/45S5 bioactive glass coating on porous titanium substrate: Influence of processing conditions and porosity parameters. *Key Eng Mater* 2016;704:343–350.
  16. Corni I, Neumann N, Novak S, König K, Veronesi P, Chen Q, Ryan MP, Boccaccini AR. Electrophoretic deposition of PEEK-nano alumina composite coatings on stainless steel. *Surf Coatings Technol* 2009;203:1349–1359.
  17. Cho J, Konopka K, Rożniatowski K, García-Lecina E, Shaffer MSP, Boccaccini AR. Characterisation of carbon nanotube films deposited by electrophoretic deposition. *Carbon N Y* 2009;47:58–67.
  18. Baştan FEFE, Atiq Ur Rehman M, YYYA, Avcu E, Üstel F, ARAR B. Electrophoretic co-deposition of PEEK-hydroxyapatite composite coatings for biomedical applications. *Colloids Surf B Biointerfaces* 2018;169:176–182.
  19. Rajeswari D, Gopi D, Ramya S, Kavitha L. Investigation of anticorrosive, antibacterial and in vitro biological properties of a sulphonated poly(etheretherketone)/strontium, cerium co-substituted hydroxyapatite composite coating developed on surface treated surgical grade stainless steel for orth. *RSC Adv* 2014;4:61525–61536.
  20. Ur Rehman MA, Ferraris S, Goldmann WH, Perero S, Bastan FE, Nawaz Q, Confiengo G, Di Ferraris M, Boccaccini AR. Antibacterial and bioactive coatings based on radio frequency co-sputtering of silver nanocluster-silica coatings on PEEK/bioactive glass layers obtained by electrophoretic deposition. *ACS Appl Mater Interfaces* 2017;9:32489–32497.
  21. Atiq M, Rehman U, Bastan FE, Nawaz Q, Boccaccini AR. Electrophoretic deposition of lawsone loaded nanoscale silicate glass/chitosan composite on PEEK/BG layers. *Electrochem Soc Trans* 2018;82:45–50.
  22. Heise S, Wirth T, Höhlinger M, Hernández YT, Ortiz JAR, Wagener V, Virtanen S, Boccaccini AR. Electrophoretic deposition of chitosan/bioactive glass/silica coatings on stainless steel and WE43 Mg alloy substrates. *Surf Coatings Technol* 2018;344:553–563.
  23. Heise S, Höhlinger M, Hernández YT, Palacio JJP, Rodríguez Ortiz JA, Wagener V, Virtanen S, Boccaccini AR. Electrophoretic deposition and characterization of chitosan/bioactive glass composite coatings on Mg alloy substrates. *Electrochim Acta* 2017;232:456–464.
  24. Heise S, Virtanen S, Boccaccini AR. Taguchi design of experiments approach to determine process parameter for the electrophoretic deposition of chitosan/bioactive glass on Mg alloy substrates. *Electrochim Soc Tras* 2018;82:81–87.
  25. Besra L, Liu M. A review on fundamentals and applications of electrophoretic deposition (EPD). *Prog Mater Sci* 2007;52:1–61.
  26. Boccaccini AR, Keim S, Ma R, Li Y, Zhitomirsky IR, Boccaccini A, Keim S, Ma R, Li Y, Zhitomirsky I, Boccaccini AR, Keim S, Ma R, Li Y, Zhitomirsky I. Electrophoretic deposition of biomaterials. *J R Soc Interface* 2010;7(Suppl 5):S581–S613.
  27. Ferrari B, Moreno R. EPD kinetics: A review. *J Eur Ceram Soc* 2010;30:1069–1078.
  28. Sarkar P, Nicholson PS. Electrophoretic deposition (EPD): Mechanisms, kinetics and application to ceramics. *J Am Ceram Soc* 1996;79:1987–2002.
  29. Biesheuvel PM, Verweij H. Theory of cast formation in electrophoretic deposition. *J Am Ceram Soc* 1999;82:1451–1455.
  30. Pishbin F, Simchi A, Ryan MP, Boccaccini AR. A study of the electrophoretic deposition of Bioglass<sup>®</sup> suspensions using the Taguchi experimental design approach. *J Eur Ceram Soc* 2010;30:2963–2970.
  31. Seuss S, Lehmann M, Boccaccini AR. Alternating current electrophoretic deposition of antibacterial bioactive glass-chitosan composite coatings. *Int J Mol Sci* 2014;15:12231–12242.
  32. Hench LL. *Bioceramics*. *J Am Ceram Soc* 1998;28:1705–1728.
  33. Seuss S, Heinloth M, Boccaccini AR. Development of bioactive composite coatings based on combination of PEEK, bioactive glass and Ag nanoparticles with antibacterial properties. *Surf Coatings Technol* 2015;301:100–105.
  34. Moskalewicz T, Seuss S, Boccaccini AR. Microstructure and properties of composite polyetheretherketone/Bioglass<sup>®</sup> coatings deposited on Ti-6Al-7Nb alloy for medical applications. *Appl Surf Sci* 2013;273:62–67.
  35. Atiq Ur Rehman M, Bastan FE, Haider B, Boccaccini AR. Electrophoretic deposition of PEEK/bioactive glass composite coatings for orthopedic implants: A design of experiments (DoE) study. *Mater Des* 2017;130:223–230.
  36. Miola M, Vernè E, Piredda A, Seuss S, Cabanas-Polo S, Boccaccini AR. Development and characterization of PEEK/B2O3-doped 45S5 bioactive glass composite coatings obtained by electrophoretic deposition. *Key Eng Mater* 2015;654:3–7.
  37. Kokubo T, Takadama H. How useful is SBF in predicting in vivo bone bioactivity? *Biomaterials*. 2006;27:2907–2915.
  38. Zhang XL, Jiang ZH, Yao ZP, Song Y, Wu ZD. Effects of scan rate on the potentiodynamic polarization curve obtained to determine the Tafel slopes and corrosion current density. *Corros Sci*. 2009;51:581–587.
  39. Simchi A, Pishbin F, Boccaccini AR. Electrophoretic deposition of chitosan. *Mater Lett* 2009;63:2253–2256.
  40. Pishbin F, Simchi A, Ryan MP, Boccaccini AR. Electrophoretic deposition of chitosan/45S5 Bioglass composite coatings for orthopaedic applications. *Surf Coatings Technol* 2011;205:5260–5268.
  41. Shi YY, Li M, Liu Q, Jia ZJ, Xu XC, Cheng Y, Zheng YF. Electrophoretic deposition of graphene oxide reinforced chitosan-hydroxyapatite nanocomposite coatings on Ti substrate. *J Mater Sci Mater Med* 2016;27:48.
  42. Mehdiipour M, Afshar A. A study of the electrophoretic deposition of bioactive glass-chitosan composite coating. *Ceram Int* 2012;38:471–476.
  43. Batmanghelich F, Ghorbani M. Effect of pH and carbon nanotube content on the corrosion behavior of electrophoretically deposited

- chitosan–hydroxyapatite–carbon nanotube composite coatings. *Ceram Int* 2013;39:5393–5402.
44. Mahmoodi S, Sorkhi L, Farrokhi-Rad M, Shahrabi T. Electrophoretic deposition of hydroxyapatite–chitosan nanocomposite coatings in different alcohols. *Surf Coatings Technol* 2013;216:106–114.
  45. Hassan WN. Phytochemical analysis of Nigerian and Egyptian henna (*Lawsonia inermis* L.) leaves using TLC, FTIR and GCMS. *Plant* 2014;2:27.
  46. Dandy LO, Oliveux G, Wood J, Jenkins MJ, Leeke GA. Accelerated degradation of polyetheretherketone (PEEK) composite materials for recycling applications. *Polym Degrad Stab* 2015;112:52–62.
  47. Pang X, Zhitomirsky I. Electrodeposition of composite hydroxyapatite–chitosan films. *Mater Chem Phys* 2005;94:245–251.
  48. Lee JH, Khang G, Lee JW, Lee HB. Interaction of different types of cells on polymer surfaces with wettability gradient. *J Colloid Interface Sci* 1998;205:323–330.
  49. Chen Q, Cordero-Arias L, Roether JA, Cabanas-Polo S, Virtanen S, Boccaccini AR. Alginate/Bioglass® composite coatings on stainless steel deposited by direct current and alternating current electrophoretic deposition. *Surf Coatings Technol* 2013;233:49–56.
  50. Nawaz Q, Atiq M, Rehman U, Burkovski A, Schmidt J, Beltrán AM, Shahid A, Alber NK, Peukert W, Boccaccini AR. Synthesis and characterization of manganese containing mesoporous bioactive glass nanoparticles for biomedical applications. *J Mater Sci Mater Med*; 2018;295
  51. Hoppe A, Meszaros R, Stähli C, Romeis S, Schmidt J, Peukert W, Marelli B, Nazhat SN, Wondraczek L, Lao J, Jallot E, Boccaccini AR. In vitro reactivity of Cu doped 45S5 Bioglass® derived scaffolds for bone tissue engineering. *J Mater Chem B* 2013;1:5659.
  52. Hench LL, Jones JR. Bioactive glasses: Frontiers and challenges. *Front Bioeng Biotechnol* 2015;3:1–12.
  53. Canal C, Pastorino D, Mestres G, Schuler P, Ginebra MP. Relevance of microstructure for the early antibiotic release of fresh and pre-set calcium phosphate cements. *Acta Biomater* 2013;9:8403–8412.
  54. Hixson AW, Crowell JH. Dependence of reaction velocity upon surface and agitation. *Ind Eng Chem Am Chem Soc* 1931;23: 1160–1168.
  55. Kopcha M, Lordi NG, Tojo KJ. Evaluation of release from selected thermosoftening vehicles. *J Pharm Pharmacol* 1991;43: 382–387.
  56. Rahmoun NM, Boucherit-Otmani Z, Boucherit K, Benabdallah M, Villemin D, Choukhou-Braham N. Antibacterial and antifungal activity of lawsone and novel naphthoquinone derivatives. *Méd Mal Infect* 2012;42:270–275.